

Toward an understanding of the properties of neural network approaches for supernovae light curve approximation

Mariia Demianenko¹, Konstantin Malanchev^{2,3}, Ekaterina Samorodova⁴, Mikhail Sysak⁵, Aleksandr Shiriaev⁶, Denis Derkach⁷, Mikhail Hushchyn⁷*

¹Max-Planck-Institut für Astronomie, Königstuhl 17, 69117 Heidelberg, Germany

²Department of Astronomy, University of Illinois at Urbana-Champaign, 1002 West Green Street, Urbana, IL 61801, USA

³Lomonosov Moscow State University, Sternberg Astronomical Institute, Universitetsky pr. 13, Moscow 119234, Russia;

⁴Lomonosov Moscow State University, Department of Mechanics and Mathematics, Leninskie gory 1, Moscow 119234, Russia;

⁵Moscow Institute of Physics and Technology, Institutskii Pereulok 9, Dolgoprudny, Moscow Region 141700, Russia;

⁶Moscow Polytechnic University, Tverskaya street, 11, Moscow 125993, Russia;

⁷HSE University, 11 Pokrovsky Bulvar, Moscow 101000, Russia;

Accepted XXX. Received YYY; in original form ZZZ

ABSTRACT

The modern time-domain photometric surveys collect a lot of observations of various astronomical objects, and the coming era of large-scale surveys will provide even more information. Most of the objects have never received a spectroscopic follow-up, which is especially crucial for transients e.g. supernovae. In such cases, observed light curves could present an affordable alternative. Time series are actively used for photometric classification and characterization, such as peak and luminosity decline estimation. However, the collected time series are multidimensional, irregularly sampled, contain outliers, and do not have well-defined systematic uncertainties. Machine learning methods help extract useful information from available data in the most efficient way. We consider several light curve approximation methods based on neural networks: Multilayer Perceptrons, Bayesian Neural Networks, and Normalizing Flows, to approximate observations of a single light curve. Tests using both the simulated PLAsTiCC and real Zwicky Transient Facility data samples demonstrate that even few observations are enough to fit networks and achieve better approximation quality than other state-of-the-art methods. We show that the methods described in this work have better computational complexity and work faster than Gaussian Processes. We analyze the performance of the approximation techniques aiming to fill the gaps in the observations of the light curves, and show that the use of appropriate technique increases the accuracy of peak finding and supernova classification. In addition, the study results are organized in a FuLu Python library available on GitHub, which can be easily used by the community.

Key words: methods: data analysis – methods: statistical – transients: supernovae – software: data analysis

1 INTRODUCTION

Time-domain photometric surveys such as the All-Sky Automated Survey (ASAS) (Pojmanski 1997), MASTER Robotic Network (Lipunov et al. 2010), the Zwicky Transient Facility (ZTF) (Bellm et al. 2019), Young Supernova Experiment (YSE) (Jones et al. 2021), and others (Drake et al. 2009; Tonry et al. 2018) collect a lot of observations of various astronomical objects. These photometric data are analysed both in near-real-time and in archives by survey teams, alert brokers (such as Antares (Matheson et al. 2021), Alerce (Förster et al. 2021) Fink (Möller et al. 2021), etc) and the community to detect, classify and characterise variable astronomical sources. Most of the objects have never get a spectroscopic, multi-wavelength or other follow-up, which especially crucial for transient such as supernova, which makes photometric classification and characterisation methods significant. The upcoming Vera C. Rubin Observatory Legacy Survey of Space and Time (LSST) (Ivezic

et al. 2019) will have 10-100 times more transient detect rate than all existing surveys all together, which only makes this problem more important.

Photometric time-series collected by ground-based optical surveys usually have following properties: 1) irregularly sampled because of seasonal factors, weather condition and survey strategy, 2) multi-dimensional if they are observed in multiple passbands, 3) having outliers caused by overlapping sources and photometric pipeline artifacts, 4) having not-well defined systematic uncertainties and underestimated stochastic uncertainties. The main challenge revealed in the era of Big Data research is how to extract useful information from the imperfect available data in the most efficient way. The application of machine learning and artificial intelligence methods is a promising solution here.

Supernovae type Ia (SN Ia) light curves are commonly used for machine learning based solutions in SN classification and characterization problems. These objects were found to be standardizable candles via the relation between their peak luminosity and luminosity decline rate (Rust 1974; Pskovskii 1977; Phillips 1993; Riess et al.

* mhushchyn@hse.ru

1996). This property of SNe Ia is widely used for luminosity distance measurements and consequent cosmological analysis (Riess et al. 1998; Perlmutter et al. 1999; Jones et al. 2019). In the upcoming era of large photometric surveys it became crucial to have a robust pipeline which finds SN Ia among other transient and variable sources, and extract its peak flux, decline rate and color.

Recently, the range of machine learning approaches for transients and variable stars classification has been presented. Participants of the Supernova Photometric Classification Challenge (Kessler et al. 2010) used many different machine-learning and classification approaches including Random Forest (RF) and Neural Network. Authors of (Richards et al. 2011) apply the RF algorithm for variable stars classification, where the light curves were represented by a set of periodic and nonperiodic features. A list of different statistical parameters such as mean, skewness, standard deviation, and kurtosis are presented in (Ferreira Lopes, C. E. & Cross, N. J. G. 2017) and (Dubath et al. 2011) for the classification using RF algorithm. (Pashchenko et al. 2017) solves the problem using SVM, Neural Networks and RF classifiers with 18 input features that describes the scatter and correlation between observations of light curves. Other similar approaches are presented in (Ball & Brunner 2010), and (Baron 2019).

Further evolution of this approach is closely related with the development of neural network models. Method proposed in (Mahabal et al. 2017) includes the transformation of the light curves into 2D histograms, where each dimension corresponds to the difference between magnitudes and timestamps for each pair of observations in the light curve. The obtained histograms are considered as images and used as input of the convolutional neural network (CNN) for model training. Similar differences are used in (Bassi et al. 2021) as inputs for the 1D CNN and Long Short Term Memory (LSTM) model for the variable star classification. Authors of (Aguirre et al. 2018) take the difference between consecutive time and magnitude values in a light curve. These vectors of differences form a 1D image with two channels and passed to 1D CNN model for solving the classification problem. Similar approach is described in (Becker et al. 2020; Möller & de Boissière 2020), where the matrix of the differences in time and magnitude are considered as sequences and used as inputs of the Recurrent Neural Network (RNN) classifier. In (Dobryakov et al. 2021) a linear interpolation of light curve values is used as well as the differences in magnitude for each consecutive pair of data points as inputs for various classification algorithms. RNN auto-encoder in (Naul et al. 2017) learns latent representation of the light curves. It then processes the curve observations as a sequence. The obtained representation is used as input of RF algorithm for object classification.

One more direction is based on the different approximation approaches of light curves and uses best-fit parameters of phenomenological functions as features for classification models. In (Bazin, G. et al. 2009), (Villar et al. 2019), and (Sánchez-Sáez et al. 2021) the light curves are approximated with specific parameterized models. The fitted parameters of these models as well as their uncertainties are used as inputs of different classification algorithms. One of the first application of neural networks for the supernovae classification based on this approach is described in (Karpenka et al. 2012). Similar model is used in (Newling et al. 2011) for classification of simulated Dark Energy Survey light curves using Boosting Decision Trees (BDTs) and Kernel Density Estimation (KDE) methods. Other functions for the light curve approximation are demonstrated in (Guy, J. et al. 2007), (Newling et al. 2011), and (Taddia, F. et al. 2015). Different parameterization methods and wavelet decomposition approach for input feature generation are presented in (Lochner et al.

2016) and tested in photometric supernova classification using a list of machine learning algorithms.

Poor approximator choice can negatively affect the classification quality and the results of the analysis. Parametric functions usually have no relation to physical processes in transients, and also have limited generalizability. It is inefficient to use this approach for datasets of objects of different types, since each class requires its own custom parametric function fit. Often, Gaussian Processes (GP) model is used in (Angus et al. 2017) as alternative for the light curves approximation in each passband. A range of various parameterization and classification approaches are considered in the Photometric LSST Astronomical Time-series Classification Challenge (PLAsTiCC) (Hložek et al. 2020). The winner of the challenge demonstrates that approximation of the light curves using GP provides better results than for other methods (Boone 2019). Currently, this approach is the state-of-the-art method for SN light-curve pre-processing (see, e.g. Qu et al. 2021; Alves et al. 2022; Burhanudin & Maund 2022 for classification and Pruzhinskaya et al. 2019; Villar et al. 2021; Ishida et al. 2021; Muthukrishna et al. 2021 for anomaly detection) and we use it as a baseline result below.

Gaussian processes is also a popular method of Supernova light curve characterization since it was used first time for the purpose of SN Ia absolute magnitude at peak standardization by Kim et al. (2013). Müller-Bravo et al. (2022) propose GP instead of commonly used light-curve templates for data-driven SN Ia fitting. (Stevance & Lee 2022) used GP-approximated light curve to get rising time and declination rate of SN Type II and IIb and study their morphology and genealogy. Authors of (Sravan et al. 2021) proposed to use 2-D Gaussian Processes for light-curve forecasting for the purpose of optimization of the follow-up strategy.

In this work, we consider different neural network models such as Multilayer Perceptron (MLP), Bayesian Neural Networks (BNN), and Normalizing Flows (NF) as an alternatives for the light curves approximation. We demonstrate that observations of a single light curve are enough to provide good quality fit results. We compare the approximation quality of the methods with the state-of-the-art approach. In addition, we explore how the models affect the indirect physical metrics: binary classification for SN Ia and the rest transient types, estimation of the light-curve peak. Since (Dobryakov et al. 2021) shows a deterioration in quality metrics when applying machine learning models to real data compared to simulation data, we test our models on both the simulated PLAsTiCC and real ZTF data samples.

We present open-source Python 3 package `Fulu`¹ implementing Neural Network light-curve approximation models described in this paper.

2 PROBLEM STATEMENT

We describe each point of a light curve by an observed flux value y_i , its error ε_i , a timestamp t_i , and a photometric passband characterised by an effective wavelength λ_i . For simplicity, let us define an input feature vector $x_i = (t_i, \lambda_i)^T$. Then, the light curve is represented by a conditional probability density distribution $p(y|x)$. Here we assume that the light flux y is a random variable, and its values y_i are sampled from the distribution:

$$y_i \sim p(y|x_i). \quad (1)$$

¹ <https://github.com/HSE-LAMBDA/fulu>

Generally, it is hard to find the distribution for a given sample, and it is not necessary for many practical cases. Thus, the goal of this work is to estimate the mean flux $\mu(x)$ and the standard deviation $\sigma(x)$ for the given x of the light curve. We use these functions for light curve interpolation. Figure 1 shows an example of a light curve for a SN Ibc from the PLAsTiCC data set, measured in the $\{u, g, r, i, z, y\}$ passbands, before and after the approximation. This problem can be solved using several machine learning algorithms. We describe a range of these models in the following section.

Flux for the ZTF catalog is defined from the magnitudes as:

$$\text{Flux [mJy]} = 10^{-0.4(m-16.4)}, \quad (2)$$

where m is ZTF magnitude. PLAsTiCC uses calibrated flux in units of FLUXCAL of SNANA (Kessler et al. 2009) having 27.5 AB-magnitude zero point. We adopted it to use the same mJy units as for the ZTF data:

$$\text{Flux [mJy]} = \text{FLUXCAL} \times 10^{-4.44}, \quad (3)$$

Time in light curves is measured in MJD.

3 APPROXIMATION METHODS

In our study, we tested various neural networks based on different ideas for the light curve approximation. The most obvious solution of the problem is to take regression models based on Multilayer Perceptrons (MLP). They learn to predict mean flux value for the given timestamp and passband. And we use two different implementations: PyTorch and scikit-learn (Pedregosa et al. 2011). PyTorch library uses computation graphs with automatic differentiation, that significantly simplifies building various models and architectures. Scikit-learn is based on NumPy arrays with manual definitions of all derivatives. It makes this library less flexible, however faster than PyTorch, which we observed in this work.

Moreover, we explored Bayesian Neural Networks (BNN), that learn optimal distributions of each weight of the model. Injecting the weight uncertainty helps to estimate the variation of the light flux predictions. In theory, BNNs are powerful predictors with interesting properties, however it is practically too hard to fit them properly. In addition, we tested Normalizing Flow (NF) as a representative of generative models. NF estimates a distribution of light curve observations. Knowing this distribution allows us to calculate the mean and variance of the light flux. The following subsections describe the details of all models used in this work.

3.1 Regression model

A simple model that can be used for the light curve approximation is a Multilayer Perceptron (MLP) for a regression task. It assumes that the flux y is normally distributed with mean $\mu(x|w)$ and constant standard deviation $\sigma(x) = \sigma$ values:

$$p(y_i|x_i, w) = \frac{1}{\sigma\sqrt{2\pi}} e^{-\frac{(y_i - \mu(x_i|w))^2}{2\sigma^2}}, \quad (4)$$

where $\mu(x_i|w)$ is estimated by the neural network with weights w . The model takes $\{x_i\}$ as inputs and learns its weights by optimizing the log-likelihood function:

$$L(w) = \frac{1}{n} \sum_{i=1}^n \log p(y_i|x_i, w) \rightarrow \max_w, \quad (5)$$

where n is the number of observations in the light curve. Let us denote the optimal weights $w_{ML} = \arg \max L(w)$. According to Section 3.1.1 in (Bishop 2006), this optimization problem is equivalent to the MSE loss minimization:

$$w_{ML} = \arg \max_w L(w) = \arg \min_w \frac{1}{n} \sum_{i=1}^n (y_i - \mu(x_i|w))^2. \quad (6)$$

Moreover, the optimal solution provides the following functions for the light curve approximation:

$$\mu(x) = \mu(x|w_{ML}), \quad (7)$$

$$\sigma(x) = \sigma = \sqrt{\frac{1}{n} \sum_{i=1}^n (y_i - \mu(x_i))^2}. \quad (8)$$

In this work, we use two MLP models implemented in two frameworks: PyTorch and scikit-learn. The PyTorch model is a one-layer neural network with 20 neurons, the activation function \tanh , which is trained with Adam optimizer. Similarly, the scikit-learn model has two layers with 20 and 10 neurons, the activation function \tanh , which is trained with the optimizer LBFSGS. LBFSGS is the second-order optimizer and converges to the optimum faster than first-order algorithms such as Adam. Further in the text and tables, these two models are designated based on the framework on which they are implemented: MLP (sklearn) and MLP (pytorch). The results, provided in the following sections show that the scikit-learn implementation is dramatically faster than other considered approximation algorithms. Example of a SN II light curve approximation is shown in Fig. 2.

3.2 Bayesian neural network

Bayesian Neural Network (BNN) uses the same observation model described in Equation 4 as the MLP models. In addition, in the BNN model it is assumed that its weights w is a random variable with distribution defined by the light curve observations $D = \{x_1, x_2, \dots, x_i, \dots, x_n\}$. Let's define a prior distribution $p(w)$ of the weights:

$$p(w) = \mathcal{N}(w|0, \alpha^2 I) = \prod_{j=1}^m \frac{1}{\alpha\sqrt{2\pi}} e^{-\frac{w_j^2}{2\alpha^2}}, \quad (9)$$

where m is the number of weights of the network and α is an adjustable parameter. Applying Bayes' rule to Equation 4 and Equation 9 we derive the posterior probability density distribution $p(w|D)$ of the BNN model's weights given the light curve observations:

$$p(w|D) \propto p(w) \prod_{i=1}^n p(y_i|x_i, w) \rightarrow \max_w, \quad (10)$$

where the objective of the model is to maximize this distribution with respect to the weights. However, it is difficult to estimate the exact expression for the prior distribution. Authors of (Blundell et al. 2015) suggest to approximate it with normal distribution $q(w)$, which has a diagonal covariance matrix Σ :

$$p(w|D) \approx q(w) = \mathcal{N}(w|\mu_w, \Sigma_w) = \prod_{j=1}^m \mathcal{N}(w_j|\mu_{w_j}, \sigma_{w_j}), \quad (11)$$

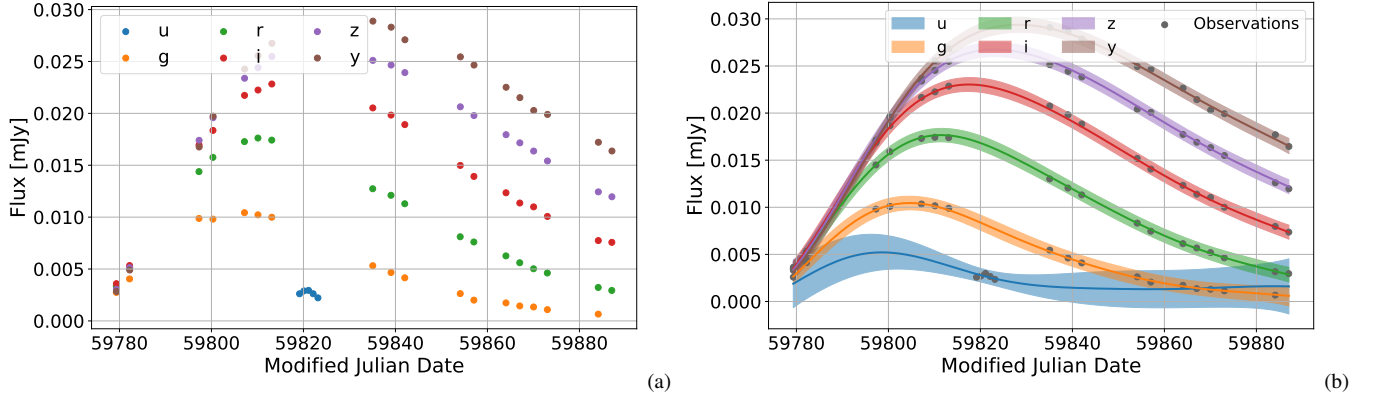


Figure 1. (a) Light curve of a PLAStiCC SN Ibc (ID 34299) before approximation. The points represent measurements in the corresponding passbands. (b) Light curve after approximation using GP method. The solid lines are the estimated mean $\mu(x)$ values. The shaded area represents $\pm 3\sigma(x)$ uncertainty band for the light curve approximation.

where μ_{w_j} and σ_{w_j} are the mean and standard deviation for a weight w_j of the BNN model. Following (Blundell et al. 2015), the optimization problem in Equation 10 is approximated by maximizing the lower variational bound:

$$L(\mu_{w_j}, \sigma_{w_j}) = \mathbb{E}_{q(w)} \left[\sum_{i=1}^n \log p(y_i | x_i, w) \right] - KL(q(w) || p(w)) \rightarrow \max_{\mu_{w_j}, \sigma_{w_j}}, \quad (12)$$

where $KL(q(w) || p(w))$ is Kullback–Leibler divergence between the distributions $q(w)$ and $p(w)$. The mean $\mu(x)$ and standard deviation $\sigma(x)$ for the light curve approximation are defined as

$$\mu(x) = \mathbb{E}_{w \sim q(w)} [\mu(x|w)], \quad (13)$$

$$\sigma(x) = \sqrt{\mathbb{V}_{w \sim q(w)} [\mu(x|w)]}. \quad (14)$$

As shown in Section 5.7.1 of (Bishop 2006), the variance of the approximation can be represented as the sum of two terms:

$$\sigma^2(x) = \sigma^2 + \sigma_{model}^2(x). \quad (15)$$

where σ^2 is the variance that arises from the intrinsic noise in the light flux y as shown in Equation 4. The second term stands for the uncertainty in the BNN model due to the uncertainty in the weights.

In this work, we use the BNN model with one linear layer of 20 neurons, and weight priors in the form of standard normal distributions $\mathcal{N}(0, 0.1)$. In such a model, the optimizer Adam and the activation function tanh are used. Example of a SN II light curve approximation is shown in Fig. 2.

3.3 Normalizing flows

Let us define a latent random variable z with the standard normal distribution $q(z) = \mathcal{N}(z|0, I)$. The goal of a Normalizing Flow (NF) model (Tabak & Turner 2013; Rezende & Mohamed 2015) is to find such an invertible function that transforms the light flux y_i into the latent variable z_i with given x_i :

$$z_i = f(y_i, x_i, w), \quad (16)$$

where w stands for the learnable parameters of the function. Then, the change of variables theorem defines the following relation between the flux $p(y_i | x_i, w)$ and the latent variable $q(z)$ distributions:

$$p(y_i | x_i, w) = q(f(y_i, x_i, w)) \left| \det \frac{\partial f(y_i, x_i, w)}{\partial y_i} \right|. \quad (17)$$

In this work, we use Real-NVP NF model (Dinh et al. 2016), where the function $f(y_i, x_i, w)$ is designed using neural networks with weights w . The optimal weights w_{ML} are estimated by maximizing the log-likelihood function:

$$L(w) = \frac{1}{n} \sum_{i=1}^n \log p(y_i | x_i, w) \rightarrow \max_w. \quad (18)$$

The main advantage of this model is that it can estimate any probability density function of the light flux $p(y_i | x_i, w)$. Then, the mean $\mu(x)$ and standard deviation $\sigma(x)$ for the light curve approximation are defined as

$$\mu(x) = \mathbb{E}_{z \sim q(z)} [f^{-1}(z, x, w_{ML})], \quad (19)$$

$$\sigma(x) = \sqrt{\mathbb{V}_{z \sim q(z)} [f^{-1}(z, x, w_{ML})]}. \quad (20)$$

We use 8 Real-NVP transformations, where two simple fully connected neural networks are used in each transformation. The model uses Adam optimizer and the tanh activation function. Example of a SN II light curve approximation is shown in Fig. 2.

3.4 Gaussian processes

Consider a light curve with observations $\{(x_1, y_1), (x_2, y_2), \dots, (x_n, y_n)\}$. GP (Williams & Rasmussen 1995) model assumes that the joint probability density function of the observations is multivariate normal with zero mean and the covariance matrix K :

$$p(Y) = \mathcal{N}(0, K), \quad (21)$$

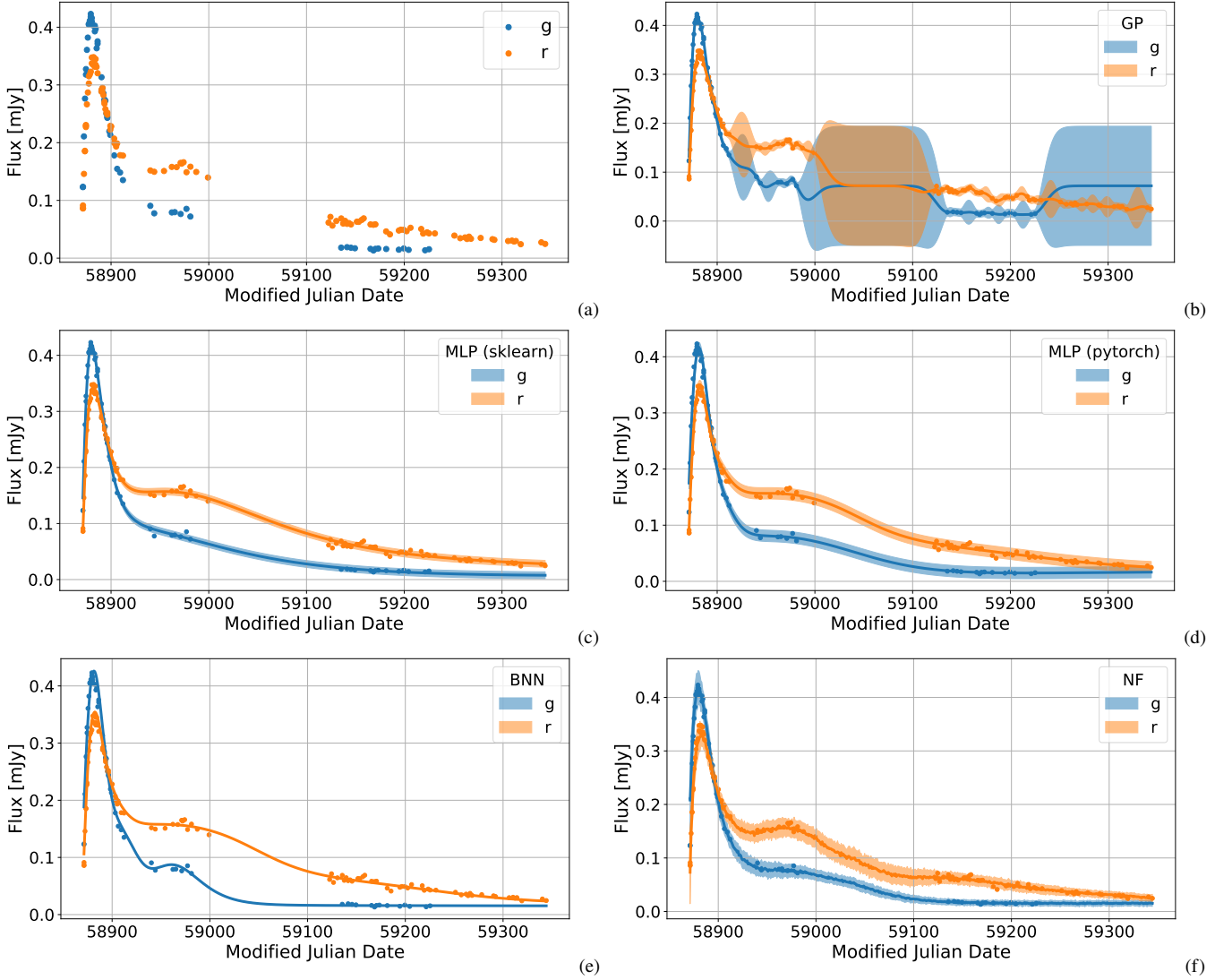


Figure 2. Examples of SN II ZTF20aahbamv light curve approximations using different methods: (a) light curve before approximation, (b) GP, (c) MLP (sklearn), (d) MLP (pytorch), (e) BNN, (f) NF. The points represent measurements in the corresponding passbands. The solid lines are the estimated mean $\mu(x)$ values. The shaded area represents $\pm \sigma(x)$ uncertainty band.

with

$$K = \begin{pmatrix} k(x_1, x_1) & \cdots & k(x_1, x_n) \\ \vdots & \ddots & \vdots \\ k(x_n, x_1) & \cdots & k(x_n, x_n) \end{pmatrix}, \quad (22)$$

where $Y = [y_1, y_2, \dots, y_n]^T$ and $k(x_i, x_j)$ is a covariance function and is considered as the model hyperparameter. In this work, we use combinations of RBF, Matern and White kernels as the covariance function. The best combination for each data set is estimated by the optimization procedure. Parameters of the kernels are estimated by maximizing the log-likelihood function:

$$L(w) = \log p(Y) = -\frac{1}{2} Y^T K^{-1} Y - \frac{1}{2} \log |K| - \frac{n}{2} \log 2\pi \rightarrow \max_w. \quad (23)$$

Using Equation 21, the joint distribution with a new pair (x, y) has the following form:

$$p(y, Y) = \mathcal{N} \left(0, \begin{pmatrix} K & K_*^T \\ K_* & K_{**} \end{pmatrix} \right), \quad (24)$$

where $K_* = [k(x, x_1), \dots, k(x, x_n)]$, and $K_{**} = k(x, x)$. Following (Williams & Rasmussen 1995), the posterior probability density function for the prediction y is also normal:

$$p(y|Y) = \mathcal{N}(y|\mu(x), \sigma(x)), \quad (25)$$

where the mean $\mu(x)$ and standard deviation $\sigma(x)$ functions are used for the light curve approximation and are defined as:

$$\mu(x) = K_* K^{-1} Y, \quad (26)$$

$$\sigma(x) = K_{**} - K_* K^{-1} K_*^T. \quad (27)$$

(Boone 2019) demonstrates that the approximation of light curves using GP provides better results than for other methods. Currently, this approach is the state-of-the-art method and we consider it as a baseline in this work. Example of a SN II light curve approximation is shown in Fig. 2.

3.5 Other models

In addition to the models described above, we also considered other regression models in machine learning such as decision trees, random forest, gradient boosting decision trees, support vector machines, and linear regression. However, the tests show bad approximation quality for these models. Thus, in this paper, we do not consider them. Moreover, we test other generative models such as Variation Autoencoders (VAE) and Generative Adversarial Networks (GAN). However, they also show bad results and are not considered here.

4 QUALITY METRICS

4.1 Approximation quality

We measure the quality of the proposed approximation methods using direct and indirect approaches. In the direct one, we measure the difference between the models' predictions and observations of light curves. In order to achieve this, the observations are divided into train and test samples using a binned split. Consider a light curve with n points $\{(x_1, y_1), (x_2, y_2), \dots, (x_n, y_n)\}$ at timestamps $\{t_1, t_2, \dots, t_n\}$, where $t_1 \leq t_2 \leq \dots \leq t_n$. Let us define the width Δt of a time bin, and split the observations into k bins $\{b_1, b_2, \dots, b_k\}$:

$$b_j = \{i : j\Delta t \leq t_i < (j+1)\Delta t\}. \quad (28)$$

We randomly select two nonempty bins b_{test} , except the first b_1 and the last b_k , to measure the approximation quality. All observations in other bins are used for the models' training. To estimate the quality, we calculate the following metrics: Root Mean Squared Error (RMSE), Mean Absolute Error (MAE), Mean Absolute Percentage Error (MAPE), Relative Squared Error (RSE) and Relative Absolute Error (RAE), which are defined as

$$\text{RMSE} = \sqrt{\frac{1}{m} \sum_{i \in b_{test}} (y_i - \mu(x_i))^2}, \quad (29)$$

$$\text{MAE} = \frac{1}{m} \sum_{i \in b_{test}} |y_i - \mu(x_i)|, \quad (30)$$

$$\text{MAPE} = \frac{100}{m} \sum_{i \in b_{test}} \left| \frac{y_i - \mu(x_i)}{y_i} \right|, \quad (31)$$

$$\text{RSE} = \sqrt{\frac{\sum_{i \in b_{test}} (y_i - \mu(x_i))^2}{\sum_{i \in b_{test}} (y_i - \bar{y})^2}}, \quad (32)$$

$$\text{RAE} = \frac{\sum_{i \in b_{test}} |y_i - \mu(x_i)|}{\sum_{i \in b_{test}} |y_i - \bar{y}|}, \quad (33)$$

where $\mu(x_i)$ is a prediction of an approximation model, m is the number of observations inside the test bins b_{test} , and \bar{y} is the average of light flux measurements y_i inside the bins.

The deviation from the true curve from the predicted one can be important in case of particular physics motivated measurement. In order to characterize the set of estimated deviations we use the following metrics to measure quality of the flux standard deviation $\sigma(x)$ estimated by the models. These metrics are the Negative Log Predictive Density (NLPD), the normalized Root Mean Squared Error based on observed error (nRMSEo), the normalized Root Mean Squared Error based on predicted error (nRMSEp) (Quiñero-Candela et al. 2006) and the Prediction Interval Coverage Probability (PICP) (Shrestha & Solomatine 2006), that are defined as

$$\text{NLPD} = \frac{1}{2} \log(2\pi) + \frac{1}{m} \sum_{i \in b_{best}} \left[\log(\sigma(x_i)) + \frac{(y_i - \mu(x_i))^2}{2\sigma(x_i)^2} \right], \quad (34)$$

$$\text{nRMSEo} = \frac{1}{m} \sum_{i \in b_{best}} \left[\frac{(y_i - \mu(x_i))^2}{2\varepsilon_i^2} \right], \quad (35)$$

$$\text{nRMSEp} = \frac{1}{m} \sum_{i \in b_{best}} \left[\frac{(y_i - \mu(x_i))^2}{2\sigma(x_i)^2} \right], \quad (36)$$

$$\text{PICP}_\alpha = \frac{1}{m} \sum_{i \in b_{best}} I \left[PL_i^L \leq y_i \leq PL_i^U \right] \times 100\%, \quad (37)$$

where ε_i is the observed flux error, PL_i^L and PL_i^U are the lower and upper prediction limits for i -th observation. The limits are symmetric and estimated based on a normal distribution $\mathcal{N}(\mu(x_i), \sigma(x_i))$ for the given coverage probability α . We calculate these metrics for each light curve and then average them over all curves in the data set. The values obtained are used as the final quality metrics of the approximation.

While the above quantities give us very good estimation of the quality of the obtained approximation, this cannot be the ultimate check. Eventually, even the best fitted model can lead to a very bad result. In order to check that these approximations do not reduce the physics value of the light curve, we solve two real-life problems: supernova classification and peak search.

4.2 Supernovae classification

In this work, we consider a quality of supernovae classification task as an indirect approach to measure the light curves approximation quality. We use approximated light curves as inputs of a Convolutional Neural Network (CNN), which is trained to separate supernovae Ia type from all others. Similarly to the direct approach, consider a light curve with n points at timestamps $\{t_1, t_2, \dots, t_n\}$, where $t_1 \leq t_2 \leq \dots \leq t_n$, and with c passbands $\{\lambda_1, \lambda_2, \dots, \lambda_c\}$. All these observations are used to fit an approximation model to estimate the $\mu(x)$ and $\sigma(x)$ functions. Then, we generate $k = 128$ new regular timestamps $\{\tau_1, \tau_2, \dots, \tau_k\}$ between t_1 and t_2 with the step $\Delta\tau = (t_n - t_1)/k$. Using the approximation function $\mu(x)$, we create the following matrix of size $(128, c)$:

$$I = \begin{pmatrix} \mu(\lambda_1, \tau_1) & \mu(\lambda_2, \tau_1) & \cdots & \mu(\lambda_c, \tau_1) \\ \mu(\lambda_1, \tau_2) & \mu(\lambda_2, \tau_2) & \cdots & \mu(\lambda_c, \tau_2) \\ \vdots & \vdots & \ddots & \vdots \\ \mu(\lambda_1, \tau_k) & \mu(\lambda_2, \tau_k) & \cdots & \mu(\lambda_c, \tau_k) \end{pmatrix}, \quad (38)$$

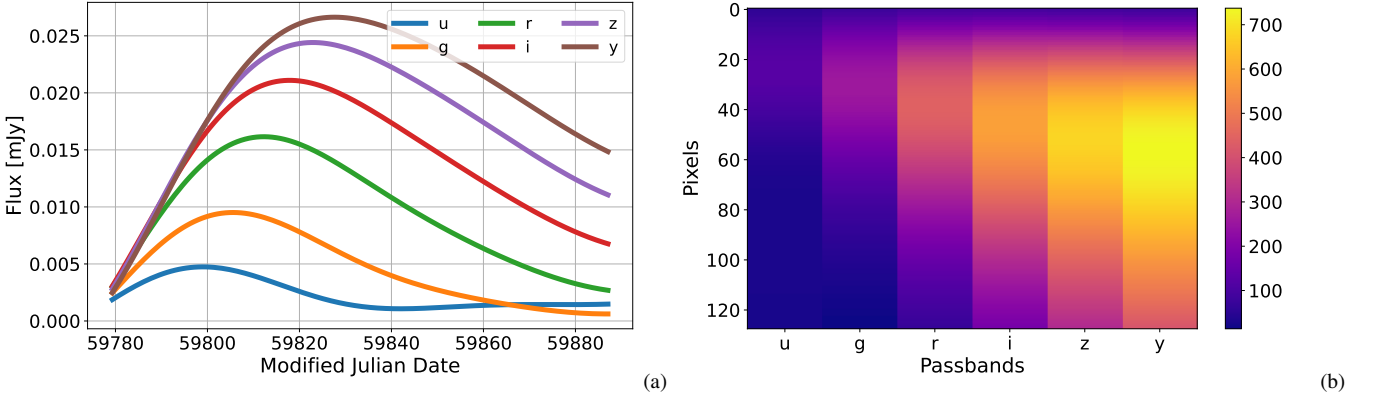


Figure 3. (a) Light curve after approximation. The solid lines are the estimated mean $\mu(x)$ values. (b) Example of a transformation of the light curve into an 1D image with 128 pixels and 6 channels, which is used as input of the CNN.

where the notation $x = (\lambda, t)$ is used. We consider this matrix I as a one-dimensional image with $k \times 1$ pixels and c channels. An example of such an image is demonstrated in Figure 3.

We used these images as inputs to a CNN classifier, which is used to separate supernova Ia types from all other types. The network contains three 1D convolutional layers with ReLU activation function, max pooling layer, and dropout followed by a fully connected layer, as shown in Figure 4. The classifier returns the probability that the image corresponds to a supernova Ia type. The model is fitted using a binary cross-entropy loss function.

Light curves in a data set are divided into train and test samples. The first one is used to train the CNN model. The test sample is used to calculate the following classification quality metrics: Area Under the ROC Curve (ROC AUC), Area Under the Precision-Recall Curve (PR AUC), Accuracy, Recall, and Precision (James et al. 2013). We use these metrics for indirect measurements of the light curve approximation quality.

4.3 Peak finding

Peak finding is an additional indirect approach of the approximation quality measurements. We use two methods to estimate the peak time stamp. In the first method, we take an image of a light curve image defined in Equation 38 and calculate the sum of light fluxes from all passbands. Then, the peak position τ_{peak} is estimated as the timestamp with the maximum total flux value:

$$\tau_{peak} = \arg \max_{\tau} \sum_i \mu(\lambda_i, \tau). \quad (39)$$

In the second method, we use a CNN regression model. It takes the light curve matrices I as inputs and predicts the peak position. Following terminology used for convolution neural networks these matrices are considered as 1D images with $k \times 1$ pixels meaning flux for each timestamp and c channels meaning passbands. The network has the same architecture as for the classification. The model is fitted using MSE loss function.

The light curves in a data set are divided into train and test samples. The first is used to train the CNN model. The test sample is used to calculate the regression quality metrics of RMSE and MAE for both of the estimation methods. We use them for indirect measurements of the light curve approximation quality.

5 PLASTICC DATASET

5.1 Approximation quality

First, we test the approximation methods on the PLAsTiCC data set (The PLAsTiCC Team et al. 2018). The dataset is produced in a simulation of the upcoming Vera C. Rubin Observatory observations. It contains simulated light curves of variable astronomical objects of different classes. The light curves are measurements of an object's photon flux in six different passbands $\{u, g, r, i, z, y\}$, which include ultra-violet, optical, and infrared regions of the light spectrum.

For our tests we select about 10,000 light curves based on the following criteria. We keep only objects with positive light flux. Also, at least 7 observations in at least 3 passbands are required. And finally, we take only light curves with breaks in measurements smaller than 50 days. Then, points of each selected light curve are spitted into train and test sets to fit and measure quality of the all approximation methods, respectively, as was described in Sec. 4.1. The optimal hyperparameter values of the methods are estimated using grid search with MAPE objective function. Obtained quality metrics values are demonstrated in Tab. 1 and Tab. 2.

The results in Tab. 1 show that MLP (sklearn) model outperforms Gaussian Processes on MAE and MAPE metrics and have the same values for RMSE. Normalizing Flows are better on RSE and RAE metrics. It demonstrates that neural networks work well on small data and can be used for light curves approximation in astronomy. The results in Tab. 2 describe ability of the methods to estimate the uncertainty of the flux measurements. Gaussian Processes show better quality metrics than other methods for all metrics except nRMSEo. Neural networks tend to underestimate the uncertainties. Normalizing Flows demonstrate the best results among neural network models.

5.2 Supernova classification

We also test the approximation methods on supernovae classification problem. For that, we take the same light curves described in the previous section and divided them into two classes. Objects with $\{90, 67, 52\}$ class names in PLAsTiCC are considered as a positive class. They are SN Ia, SN Ia-91bg and SN Iax supernova types respectively. All other objects are considered as a negative class.

We use the approximation methods for light curve augmentation and transforming them into 1D images with 6 channels as it is described in Section 4.2. Here we use the same optimal hyperparameter values estimated in the previous section. The images are feed into

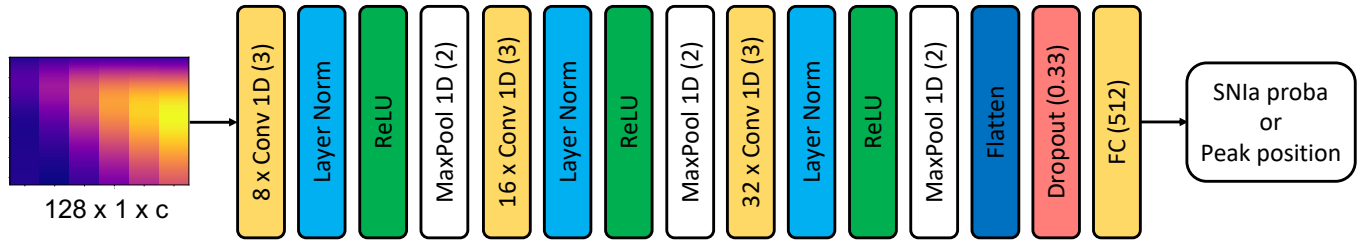


Figure 4. Architecture of the CNN model for supernovae type classification and peak estimation.

Table 1. Regression quality metrics for approximation models on PLAsTiCC. Mean flux estimation quality.

Model	RMSE, μJy	MAE, μJy	RSE	RAE	MAPE
GP	3.5 ± 0.3	2.8 ± 0.3	1.2 ± 0.1	1.1 ± 0.1	19.9 ± 0.3
MLP (sklearn)	3.5 ± 0.3	2.8 ± 0.3	1.2 ± 0.1	1.1 ± 0.1	17.9 ± 0.2
MLP (pytorch)	3.8 ± 0.4	3.1 ± 0.3	1.3 ± 0.2	1.2 ± 0.1	21.6 ± 0.3
BNN	4.2 ± 0.3	3.4 ± 0.3	1.6 ± 0.3	1.5 ± 0.2	26.4 ± 0.3
NF	3.6 ± 0.4	2.8 ± 0.3	1.1 ± 0.1	1.03 ± 0.09	18.5 ± 0.3

Table 2. Regression quality metrics for approximation models PLAsTiCC. Flux uncertainty estimation quality.

Model	NLPD	nRMSEo	nRMSEp	PICP ₆₈ , %	PICP ₉₅ , %
GP	5.25 ± 0.09	6.6 ± 0.1	1.26 ± 0.01	67.5 ± 0.3	86.5 ± 0.2
MLP (sklearn)	20 ± 2	6.4 ± 0.1	3.33 ± 0.05	45.6 ± 0.3	65.4 ± 0.3
MLP (pytorch)	18 ± 1	7.6 ± 0.1	3.25 ± 0.04	45.1 ± 0.3	64.8 ± 0.3
BNN	26.4 ± 0.3	9.1 ± 0.1	2.04 ± 0.02	51.9 ± 0.3	73.7 ± 0.3
NF	10.9 ± 0.7	6.5 ± 0.1	2.05 ± 0.03	56.3 ± 0.3	80.8 ± 0.3

CNN for the classification. About 60% of the light curves are used to train the CNN, and other 40% are used to estimate the classification quality. The metric values are demonstrated in Tab. 3.

The results show that Gaussian Processes are the best based on the all quality metrics. Normalizing flows hold the second place with differences from the GP model within the uncertainty values. In general, all methods demonstrate similar results. We conclude, that the choice of the approximation method does not have significant impact on the supernovae classification results.

5.3 Peak finding

For the peak finding test we take only objects of SN Ia type. Similarly to the classification task, we use the approximation methods to convert light curves into 1D images. Then, we use them to estimate time of peaks using two approaches considered in Section 4.3: direct and CNN based. About 60% of the light curves are used to train the CNN, and other 40% are used to estimate the peak finding quality. Quality metric values are demonstrated in Tab. 4 and Tab. 5.

Tab. 4 shows that GP model has better results for the direct approach, than the neural network-based approximation methods. Tab. 5 shows that CNN helps reduce the error of the peak prediction more than twice depending on the approximation methods. In this case, the best results are for the MLP method (sklearn) and the GP model on the second place.

6 ZTF OBSERVATIONS

6.1 Approximation quality

The Zwicky Transient Facility (ZTF) scans the entire visible northern sky with a cadence of 3 days. The ZTF Bright Transient Survey (BTS) (Fremling et al. 2019) is a major spectroscopic project that complements the ZTF photometric survey. The objective of BTS is to spectroscopically classify extra-galactic transients with $m_{peak} \leq 18.5\text{mag}$ in ZTF $\{g, r\}$ passbands, and publicly announce these classifications. BTS transient discoveries are predominantly supernovae. It is the largest flux-limited SN exploration to date.

The ANTARES data broker (Matheson et al. 2021) was used to download the light curves of the ZTF Bright Transient Survey catalog. With the help of this broker, light curves were downloaded from the ZTF release date by the names of objects from the Bright Transient Survey. To test the models, all light curves of objects presented in ZTF BTS at the time of 23:29 09/22/2021 were downloaded.

For the approximation method tests, we keep only objects with at least 10 observations in $\{g, r\}$ passbands. The total number of selected light curves is 1870. Then, points of each light curve are splitted into train and test sets to fit and measure quality of all approximation methods, respectively, as it was described in Sec. 4.1. The optimal hyperparameter values of the methods are estimated using grid search with MAPE objective function. Quality metric values are demonstrated in Tab. 6 and Tab. 7.

The results in Tab. 6 show that MLP (sklearn) model outperforms Gaussian Processes on RAE and MAPE metrics, and have the same values for RMSE, MAE and RSE. It demonstrates that neural

Table 3. Supernovae classification quality metrics for approximation models on PLAsTiCC.

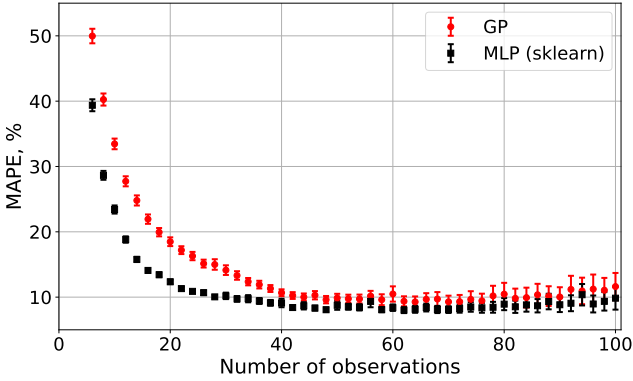
Model	ROC AUC	PR AUC	Log Loss	Accuracy	Recall	Precision
GP	0.996 ± 0.001	0.993 ± 0.001	0.078 ± 0.007	0.975 ± 0.002	0.961 ± 0.005	0.964 ± 0.005
MLP (sklearn)	0.993 ± 0.001	0.986 ± 0.002	0.10 ± 0.01	0.970 ± 0.003	0.952 ± 0.006	0.959 ± 0.005
MLP (pytorch)	0.993 ± 0.001	0.988 ± 0.002	0.100 ± 0.008	0.968 ± 0.003	0.960 ± 0.005	0.948 ± 0.006
BNN	0.994 ± 0.001	0.988 ± 0.002	0.092 ± 0.007	0.970 ± 0.003	0.956 ± 0.005	0.954 ± 0.005
NF	0.995 ± 0.001	0.992 ± 0.001	0.083 ± 0.008	0.973 ± 0.002	0.957 ± 0.005	0.963 ± 0.005

Table 4. Peak finding quality metrics for approximation models on PLAsTiCC. Direct approach: peak is determined using the sum of all passbands.

Model	RMSE, days	MAE, days	RSE	RAE	MAPE, %
GP	3.14 ± 0.09	2.04 ± 0.04	0.0102 ± 0.0003	0.0075 ± 0.0002	0.0034 ± 0.0001
MLP (sklearn)	4.2 ± 0.1	2.67 ± 0.06	0.0136 ± 0.0003	0.0098 ± 0.0003	0.0044 ± 0.0001
MLP (pytorch)	5.4 ± 0.1	3.61 ± 0.07	0.0174 ± 0.0004	0.0133 ± 0.0003	0.0060 ± 0.0001
BNN	6.1 ± 0.1	4.39 ± 0.08	0.0199 ± 0.0004	0.0162 ± 0.0004	0.0073 ± 0.0001
NF	5.8 ± 0.1	3.95 ± 0.08	0.0188 ± 0.0004	0.0146 ± 0.0004	0.0066 ± 0.0001

Table 5. Peak finding quality metrics for approximation models on PLAsTiCC. CNN based approach: CNN is trained to predict the true peak position.

Model	RMSE, days	MAE, days	RSE	RAE	MAPE, %
GP	1.76 ± 0.07	1.22 ± 0.04	0.0057 ± 0.0002	0.0045 ± 0.0002	0.00202 ± 0.00006
MLP (sklearn)	1.67 ± 0.06	1.15 ± 0.04	0.0054 ± 0.0002	0.0042 ± 0.0002	0.00192 ± 0.00006
MLP (pytorch)	1.9 ± 0.1	1.26 ± 0.04	0.0061 ± 0.0004	0.0047 ± 0.0002	0.00210 ± 0.00007
BNN	1.99 ± 0.08	1.34 ± 0.04	0.0064 ± 0.0003	0.0049 ± 0.0002	0.00223 ± 0.00009
NF	2.17 ± 0.09	1.51 ± 0.05	0.0070 ± 0.0003	0.0056 ± 0.0002	0.00251 ± 0.00008


Figure 5. Dependence of MAPE approximation quality metric on the number of observations in a ZTF light curve for GP and MLP (sklearn) methods. The horizontal axis shows how many observations were used to fit each method. The number of light curves in our sample drops with increasing the number of observations. Error bars show uncertainty of MAPE measurements.

networks work well on real data and can be used for light curve approximation in ZTF.

As in case of simulation, we quantify the ability of the methods to estimate the uncertainty of the flux measurements in Tab. 7. As can be judged from the table, Normalizing Flows show better quality metrics than other methods for all metrics except nRMSE and PICP₆₈. Gaussian Processes demonstrate similar results. In general, neural networks tend to underestimate the uncertainties on ZTF as well as on PLAsTiCC.

We conduct an additional experiment to measure the dependency of the approximation quality from the number of observations in a light curve. We split each light curve in our ZTF data set into train and test samples. The test sample contains points from two time bins with a width of 5 days. We use them to calculate the MAPE metric values. From the train sample we randomly select N observations from the light curve for the approximation fitting. If there is a lack of points, the curve is discarded. We estimate the MAPE mean value and its uncertainty using bootstrap technique over the selected light curves. This procedure is repeated for N from 6 to 100 observations with a step of 2. The results are demonstrated in Fig. 5. As expected, the plot shows that the approximation error significantly drops with increase of the number of observations. The dependencies flatten after number of training points pass 50. MLP method shows better approximation quality than GP in all ranges of N . We conclude that neural networks work well even with a very small number of observations in a light curve.

6.2 Supernova classification

We continue with test of the approximation methods on the supernovae classification problem. For that, we take the same light curves described in the previous section and divide them into two classes. Objects of SN Ia, SN Ia-91T, SN Ia-pec, SN Ia-91bg, SN Iax, and SN Ia-CSM supernova types are considered as a positive class. All other objects are considered as a negative class.

We use the approximation methods for light curve augmentation and transform them into 1D images with 2 channels as it is described in Section 4.2. Here we use the same optimal hyperparameter values estimated in the previous section. Images are fed into CNN for

Table 6. Regression quality metrics for approximation models on ZTF. Mean flux estimation quality.

Model	RMSE, mJy	MAE, mJy	RSE	RAE	MAPE, %
GP	0.018 ± 0.002	0.015 ± 0.002	0.66 ± 0.04	0.66 ± 0.04	11.0 ± 0.3
MLP (sklearn)	0.018 ± 0.001	0.015 ± 0.001	0.66 ± 0.05	0.65 ± 0.05	9.9 ± 0.2
MLP (pytorch)	0.019 ± 0.001	0.015 ± 0.001	0.68 ± 0.05	0.66 ± 0.05	10.4 ± 0.3
BNN	0.021 ± 0.001	0.018 ± 0.001	0.77 ± 0.06	0.75 ± 0.06	11.4 ± 0.3
NF	0.021 ± 0.002	0.017 ± 0.001	0.72 ± 0.05	0.72 ± 0.05	10.6 ± 0.2

Table 7. Regression quality metrics for approximation models ZTF. Flux uncertainty estimation quality.

Model	NLPD	nRMSEo	nRMSEp	PICP ₆₈ , %	PICP ₉₅ , %
GP	-2.57 ± 0.05	1.10 ± 0.03	1.16 ± 0.02	65.7 ± 0.6	88.4 ± 0.5
MLP (sklearn)	3.4 ± 0.6	1.07 ± 0.03	2.64 ± 0.07	45.7 ± 0.7	68.0 ± 0.7
MLP (pytorch)	8 ± 2	1.13 ± 0.03	2.99 ± 0.09	44.7 ± 0.7	65.8 ± 0.7
BNN	66 ± 6	1.25 ± 0.03	7.9 ± 0.2	19.7 ± 0.5	35.4 ± 0.7
NF	-2.61 ± 0.05	1.19 ± 0.03	0.86 ± 0.02	79.0 ± 0.6	94.4 ± 0.4

classification. About 60% of the light curves are used to train the CNN, and other 40% are used to estimate the classification quality. The metric values are demonstrated in Tab. 8.

The results show that all methods demonstrate similar results. We conclude that choosing the approximation method does not have significant impact on the supernovae classification results.

6.3 Peak finding

Similarly to the classification task, we approximate light curves into a regular high-cadence time grid. Then, we use them to estimate time of peaks using direct approach considered in Section 4.3. Examples of ZTF light curves with estimated peaks are shown in Fig. 6. Table 9 shows peak positions and magnitudes of the BTS ZTF objects.

7 CONCLUSION

This work shows the results of light curves approximation using neural networks on the PLAsTiCC and ZTF data sets. The outcomes help to conclude the following statements:

- Neural Network trained on a single light curve is a reasonable alternative to other approximation methods. This approach is suitable for both single-object and catalog-level studies.
- Neural Networks require $O(N)$ operations for the approximation fitting, compared to $O(N^3)$ for GP method, where N is the number of observations in a light curve. The real computational time significantly depends on specific implementations of the methods. We recommend to use LBFGS optimizer for any model.
- Approximation models can be used to generate additional observations for the light curves. These synthetic observations help to estimate various physical properties of the astronomical objects, such as peak time and supernova type.
- Supernova type identification and peak finding using CNNs does not show dependence from the approximation methods. Neural Networks and GP demonstrate similar qualities.
- FuLu Python library for light-curve approximation which implements Neural Network methods for light curves with virtually any number of observations in a curve is presented.

ACKNOWLEDGEMENT

KM work on data preparation is supported by the RFBR and CNRS according to the research project No. 21-52-15024. DD, MH and MD are supported by the HSE Basic Research Fund in the design, construction, and testing of data augmentation techniques. MD acknowledge the RScF grant No. 19-12-00281. We express our appreciation to Matvey Volkov, who developed a website for visualizing results of this paper.

Facilities: this research was supported in part through computational resources of HPC facilities at HSE University (Kostenetskiy et al. 2021).

DATA AVAILABILITY

Python library is available in the GitHub repository FuLu². Scripts of all our experiments in this work are provided in the GitHub repository³ as well. It also contains five CSV tables with results of peak estimation experiments for BTS ZTF for different approximation models. The website with interactive plots for approximation experiments on BTS ZTF⁴ can help to understand which model is more useful for objects in this catalog.

² <https://github.com/HSE-LAMBDA/fulu>

³ https://github.com/HSE-LAMBDA/light_curve_approx

⁴ <http://lc-dev.voxastro.org/>

Table 8. Supernovae classification quality metrics for approximation models on ZTF.

Model	ROC AUC	PR AUC	Log Loss	Accuracy	Recall	Precision
GP	0.94 ± 0.01	0.976 ± 0.008	0.26 ± 0.03	0.90 ± 0.02	0.95 ± 0.01	0.92 ± 0.02
MLP (sklearn)	0.95 ± 0.01	0.981 ± 0.005	0.26 ± 0.04	0.90 ± 0.02	0.93 ± 0.02	0.93 ± 0.01
MLP (pytorch)	0.96 ± 0.01	0.983 ± 0.005	0.29 ± 0.05	0.90 ± 0.02	0.93 ± 0.02	0.93 ± 0.01
BNN	0.95 ± 0.01	0.980 ± 0.006	0.31 ± 0.05	0.89 ± 0.02	0.91 ± 0.02	0.94 ± 0.02
NF	0.94 ± 0.01	0.97 ± 0.01	0.39 ± 0.07	0.89 ± 0.02	0.91 ± 0.02	0.94 ± 0.01

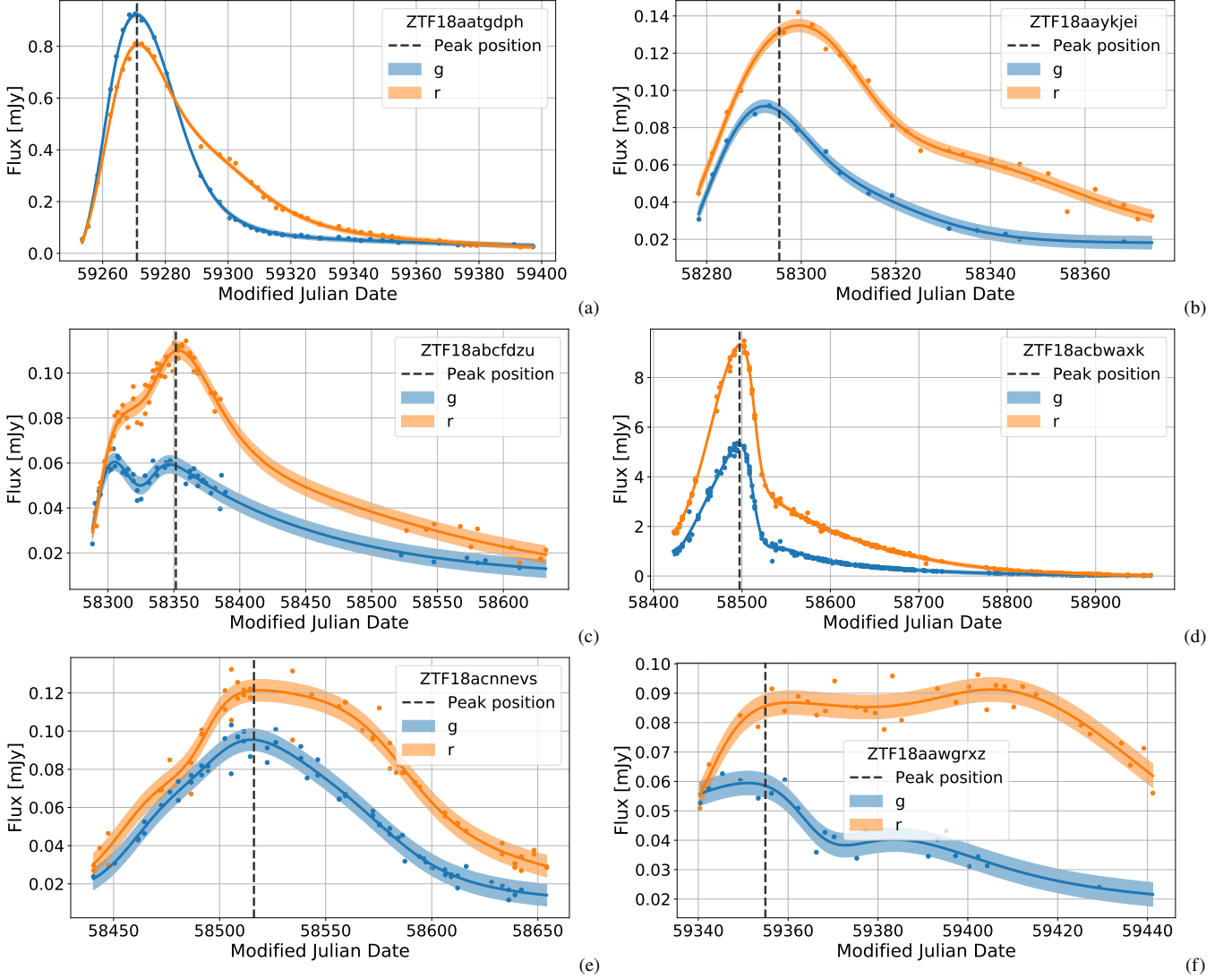

Figure 6. Examples of peak direct estimation using MLP (sklearn) approximations for a range of ZTF objects: (a) ZTF18aatgdph, (b) ZTF18aaykjei, (c) ZTF18abcfdz, (d) ZTF18acbwaxk, (e) ZTF18acnnevs, (f) ZTF18aawgrxz. The points represent measurements in the corresponding passbands. The solid lines are the estimated mean $\mu(x)$ values. The shaded area represents $\pm\sigma(x)$ uncertainty band.

Table 9. Estimated peaks for ZTF objects. Approximated using MLP (sklearn) model. The full version is available online.

ZTF name	SN name	m_g	t_g	m_r	t_r	m_Σ	t_Σ
ZTF21abwxaht	SN 2021xqc	18.71	59469.60250	18.52	59471.90505	17.87	59470.37001
ZTF21abjrwhq	SN 2021sdv	18.25	59410.74629	18.17	59411.12950	17.46	59411.12950
ZTF21abcgaln	SN 2021mxx	16.55	59363.71318	16.16	59366.15413	15.60	59364.93366
ZTF21aafvpg	SN 2021jap	17.01	59330.54799	17.14	59332.12218	16.32	59331.07272
ZTF21aapkfx	SN 2021fqh	16.91	59301.93222	16.98	59301.93222	16.19	59301.93222
ZTF21aagqcnl	SN 2021biz	15.71	59258.66084	15.83	59258.66084	15.02	59258.66084
ZTF20acwfvx	SN 2020acaf	18.57	59198.98497	18.62	59200.19335	17.84	59199.79055
ZTF20acobevy	SN 2020yub	18.25	59158.45014	18.32	59160.87008	17.54	59159.41812
ZTF20acedqis	SN 2020ufx	18.24	59122.09822	18.30	59126.93300	17.59	59125.72430
ZTF20abuqali	SN 2020rht	19.04	59080.45034	18.99	59080.45034	18.26	59080.45034
ZTF20abhlnz	SN 2020nke	18.96	59035.17439	18.74	59038.62660	18.12	59036.32513
ZTF20aayjxdv	SN 2020jge	18.10	58986.15285	18.16	58987.64490	17.38	58986.89887
ZTF20aakbtyz	SN 2020bjg	18.64	58888.80773	18.68	58889.20067	17.91	58888.80773
ZTF19acxyumq	SN 2019wvc	16.79	58844.91564	16.87	58844.91564	16.08	58844.91564
ZTF19abyjjxp	SN 2019qcj	16.97	58746.44892	16.87	58746.44892	16.17	58746.44892
ZTF19abhzelh	SN 2019lrv	17.67	58701.41276	17.73	58702.18964	16.95	58701.41276
ZTF19aaugaam	SN 2019evh	17.95	58623.55538	18.01	58637.28421	17.27	58626.78569
ZTF19aadnxog	SN 2019vb	16.71	58514.63476	16.66	58521.57320	15.96	58516.36937
ZTF18abdfydj	SN 2018dzt	18.30	58310.05330	18.69	58308.08598	17.73	58309.39752
ZTF18aatgdph	SN 2021cgl	16.49	59270.91968	16.63	59272.37189	15.81	59270.91968
ZTF18aaykjei	SN 2018crl	19.02	58292.80533	18.57	58299.58256	18.04	58295.70986
ZTF18abcfzdu	SN 2018dfa	19.45	58305.60431	18.79	58354.25815	18.33	58350.78288
ZTF18acbwaxk	SN 2018hna	14.56	58494.24002	13.99	58499.68246	13.49	58494.24002
ZTF18acnnevs	SN 2018lng	18.98	58516.02974	18.67	58526.82415	18.07	58520.3475
ZTF18aawgrxz	SN 2021lmp	19.47	59349.49727	19.0	59405.52445	18.51	59354.59065

REFERENCES

- Aguirre C., Pichara K., Becker I., 2018, *Monthly Notices of the Royal Astronomical Society*, 482, 5078
- Alves C. S., Peiris H. V., Lochner M., McEwen J. D., Allam T., Biswas R., LSST Dark Energy Science Collaboration 2022, *ApJS*, 258, 23
- Angus R., Morton T., Aigrain S., Foreman-Mackey D., Rajpaul V., 2017, *Monthly Notices of the Royal Astronomical Society*, 474, 2094
- Ball N. M., Brunner R. J., 2010, *International Journal of Modern Physics D*, 19, 1049
- Baron D., 2019, Machine Learning in Astronomy: a practical overview ([arXiv:1904.07248](https://arxiv.org/abs/1904.07248))
- Bassi S., Sharma K., Gomekar A., 2021, *Frontiers in Astronomy and Space Sciences*, 8
- Bazin, G. et al., 2009, *A&A*, 499, 653
- Becker I., Pichara K., Catelan M., Protopapas P., Aguirre C., Nikzat F., 2020, *Monthly Notices of the Royal Astronomical Society*, 493, 2981
- Bellm E. C., et al., 2019, *Publications of the Astronomical Society of the Pacific*, 131, 068003
- Bishop C. M., 2006, *Pattern Recognition and Machine Learning (Information Science and Statistics)*. Springer-Verlag, Berlin, Heidelberg
- Blundell C., Cornebise J., Kavukcuoglu K., Wierstra D., 2015, Weight Uncertainty in Neural Networks ([arXiv:1505.05424](https://arxiv.org/abs/1505.05424))
- Boone K., 2019, *The Astronomical Journal*, 158, 257
- Burhanudin U. F., Maund J. R., 2022, arXiv e-prints, p. [arXiv:2208.01328](https://arxiv.org/abs/2208.01328)
- Dinh L., Sohl-Dickstein J., Bengio S., 2016, arXiv e-prints, p. [arXiv:1605.08803](https://arxiv.org/abs/1605.08803)
- Dobryakov S., Malanchev K., Derkach D., Hushchyn M., 2021, *Astronomy and Computing*, 35, 100451
- Drake A. J., et al., 2009, *The Astrophysical Journal*, 696, 870
- Dubath P., et al., 2011, *Monthly Notices of the Royal Astronomical Society*, 414, 2602
- Ferreira Lopes, C. E. Cross, N. J. G. 2017, *A&A*, 604, A121
- Förster F., et al., 2021, *AJ*, 161, 242
- Fremling U. C., et al., 2019, The Zwicky Transient Facility Bright Transient Survey I: Spectroscopic Classification and the Redshift Completeness of Local Galaxy Catalogs, [doi:10.48550/ARXIV.1910.12973](https://arxiv.org/abs/1910.12973), <https://arxiv.org/abs/1910.12973>
- Guy, J. et al., 2007, *A&A*, 466, 11
- Hložek R., et al., 2020, Results of the Photometric LSST Astronomical Time-series Classification Challenge (PLAsTiCC) ([arXiv:2012.12392](https://arxiv.org/abs/2012.12392))
- Ishida E. E. O., et al., 2021, *A&A*, 650, A195
- Ivezić Ž., et al., 2019, *ApJ*, 873, 111
- James G., Witten D., Hastie T., Tibshirani R., 2013, *An Introduction to Statistical Learning: with Applications in R*. Springer, <https://faculty.marshall.usc.edu/gareth-james/ISL/>
- Jones D. O., et al., 2019, *ApJ*, 881, 19
- Jones D. O., et al., 2021, *ApJ*, 908, 143
- Karpenka N. V., Feroz F., Hobson M. P., 2012, *Monthly Notices of the Royal Astronomical Society*, 429, 1278
- Kessler R., et al., 2009, *PASP*, 121, 1028
- Kessler R., et al., 2010, *Publications of the Astronomical Society of the Pacific*, 122, 1415
- Kim A. G., et al., 2013, *ApJ*, 766, 84
- Kostenetskiy P. S., Chulkevich R. A., Kozyrev V. I., 2021, *Journal of Physics: Conference Series*, 1740, 012050
- Lipunov V., et al., 2010, *Advances in Astronomy*, 2010, 349171
- Lochner M., McEwen J. D., Peiris H. V., Lahav O., Winter M. K., 2016, *The Astrophysical Journal Supplement Series*, 225, 31
- Mahabal A., Sheth K., Gieseke F., Pai A., Djorgovski S. G., Drake A. J., Graham M. J., 2017, in 2017 IEEE Symposium Series on Computational Intelligence (SSCI), pp 1–8, [doi:10.1109/SSCI.2017.8280984](https://doi.org/10.1109/SSCI.2017.8280984)
- Matheson T., et al., 2021, *AJ*, 161, 107
- Möller A., de Boissière T., 2020, *MNRAS*, 491, 4277
- Möller A., et al., 2021, *MNRAS*, 501, 3272
- Müller-Bravo T. E., Sullivan M., Smith M., Frohmaier C., Gutiérrez C. P., Wiseman P., Zontou Z., 2022, *MNRAS*, 512, 3266
- Muthukrishna D., Mandel K. S., Lochner M., Webb S., Narayan G., 2021, arXiv e-prints, p. [arXiv:2112.08415](https://arxiv.org/abs/2112.08415)
- Naul B., Bloom J. S., Pérez F., van der Walt S., 2017, *Nature Astronomy*, 2, 151–155
- Newling J., et al., 2011, *Monthly Notices of the Royal Astronomical Society*, 414, 1987
- Pashchenko I. N., Sokolovsky K. V., Gavras P., 2017, *Monthly Notices of the Royal Astronomical Society*, 475, 2326
- Pedregosa F., et al., 2011, *Journal of Machine Learning Research*, 12, 2825
- Perlmutter S., et al., 1999, *ApJ*, 517, 565
- Phillips M. M., 1993, *ApJ*, 413, L105

- Pojmanski G., 1997, *Acta Astron.*, **47**, 467
- Pruzhinskaya M. V., Malanchev K. L., Kornilov M. V., Ishida E. E. O., Mondon F., Volnova A. A., Korolev V. S., 2019, *MNRAS*, **489**, 3591
- Pskovskii I. P., 1977, *Soviet Ast.*, **21**, 675
- Qu H., Sako M., Möller A., Doux C., 2021, *AJ*, **162**, 67
- Quiñonero-Candela J., Rasmussen C., Sinz F., Bousquet O., Schölkopf B., 2006, *Evaluating Predictive Uncertainty Challenge*. Springer, pp 1–27, doi:10.1007/11736790_1
- Rezende D., Mohamed S., 2015, in Bach F., Blei D., eds, *Proceedings of Machine Learning Research Vol. 37, Proceedings of the 32nd International Conference on Machine Learning*. PMLR, Lille, France, pp 1530–1538, <https://proceedings.mlr.press/v37/rezende15.html>
- Richards J. W., et al., 2011, *The Astrophysical Journal*, **733**, 10
- Riess A. G., Press W. H., Kirshner R. P., 1996, *ApJ*, **473**, 88
- Riess A. G., et al., 1998, *AJ*, **116**, 1009
- Rust B. W., 1974, PhD thesis, Oak Ridge National Laboratory, Tennessee
- Sánchez-Sáez P., et al., 2021, *AJ*, **161**, 141
- Shrestha D. L., Solomatine D. P., 2006, *Neural Networks*, **19**, 225
- Pravna N., Graham M. J., Fremling C., Coughlin M. W., 2021, arXiv e-prints, p. arXiv:2112.05897
- Stevance H. F., Lee A., 2022, arXiv e-prints, p. arXiv:2206.14816
- Tabak E. G., Turner C. V., 2013, *Communications on Pure and Applied Mathematics*, **66**, 145
- Taddia, F. et al., 2015, *A&A*, **574**, A60
- The PLAsTiCC Team et al., 2018, *The Photometric LSST Astronomical Time-series Classification Challenge (PLAsTiCC): Data set*, doi:10.48550/ARXIV.1810.00001, <https://arxiv.org/abs/1810.00001>
- Tonry J. L., et al., 2018, *PASP*, **130**, 064505
- Villar V. A., et al., 2019, *ApJ*, **884**, 83
- Villar V. A., Cranmer M., Berger E., Contardo G., Ho S., Hosseinzadeh G., Lin J. Y.-Y., 2021, *ApJS*, **255**, 24
- Williams C., Rasmussen C., 1995, *Gaussian Processes for Regression*, <https://proceedings.neurips.cc/paper/1995/file/7cce53cf90577442771720a370c3c723-Paper.pdf>

This paper has been typeset from a $\text{\TeX}/\text{\LaTeX}$ file prepared by the author.